



## Ocean Phosphorus Inventory and Ocean Deoxygenation: Large Uncertainties in Future Projections on Millennial Timescales

5 Tronje P. Kemena<sup>1</sup>, Andreas Oschlies<sup>1</sup>, Wolfgang Koeve<sup>1</sup>, Klaus Wallmann<sup>1</sup>, Angela Landolfi<sup>1</sup>,  
Andrew W. Dale<sup>1</sup>

<sup>1</sup>GEOMAR Helmholtz Centre for Ocean Research Kiel, Düsterbrooker Weg 20,  
24105, Kiel

*Correspondence to:* Tronje P. Kemena (tkemena@geomar.de)

### Abstract

10 Previous studies have suggested that weathering and benthic phosphorus (P) fluxes, triggered by  
climate warming, can increase the oceanic P inventory on millennial time scales, promoting ocean  
productivity and deoxygenation. In this study, we assessed the major uncertainties in projected P  
inventories and their imprint on ocean deoxygenation using an Earth system model of intermediate  
15 complexity for a business-as-usual carbon dioxide (CO<sub>2</sub>) emission scenario until year 2300 and  
subsequent linear decline to zero emissions until year 3000.

Model results suggest a large spread in the simulated oceanic P inventory due to uncertainties in (1)  
assumptions for weathering parameters, (2) the representation of bathymetry on slopes and shelves in  
the model bathymetry, (3) the parametrization of benthic P fluxes and (4) the representation of  
20 sediment P inventories. Our best estimate for changes in the global ocean P inventory by the year 5000  
caused by global warming amounts to +30% compared to pre-industrial levels. Weathering, benthic  
and anthropogenic fluxes of P contributed +25%, +3% and +2% respectively. The total range of  
oceanic P inventory changes across all model simulations varied between +2% and +60%. Suboxic  
volumes were up to 5 times larger than in a model simulation with a constant oceanic P inventory.  
25 Considerably large amounts of the additional P left the ocean surface unused by phytoplankton via  
physical transport processes as preformed P. Nitrogen fixation was not able to adjust the oceanic  
nitrogen inventory to the increasing P levels or to compensate for the nitrogen loss due to increased  
denitrification. This is in contrast to palaeo reconstructions of large-scale deoxygenation events.

We suggest that uncertainties in P weathering, nitrogen fixation and benthic P feedbacks need to be  
reduced to achieve more reliable projections of oceanic deoxygenation on millennial timescales.

### 30 1 Introduction

Oceanic phosphorus (P) inventories are known to substantially affect oceanic oxygen inventories on  
millennial timescales (Tsandev and Slomp, 2009; Palastanga et al., 2011; Monteiro et al., 2012).  
Phosphorus is considered the ultimate limiting nutrient for ocean productivity at the global scale  
(Tyrrell, 1999). Elevated supply of P to the ocean stimulates production and export of organic matter  
35 and deoxygenation, which possibly drives more intense oxygen depletion in the oxygen deficient zones  
and along the continental margins, with release of additional P from sediments turning anoxic (Van



Cappellen and Ingall, 1994; Palastanga et al., 2011). Such a positive feedback was discussed for a global warming scenario under present-day conditions (Niemeyer et al., 2017) as well as for large-scale deoxygenation events in the Cretaceous era, the so-called oceanic anoxic events (OAEs) (Tsandev and  
40 Slomp, 2009; Monteiro et al., 2012; Ruvalcaba Baroni et al., 2014). For the Cretaceous, it has been suggested that atmospheric carbon dioxide (CO<sub>2</sub>) concentrations as high as 1000 to 3000 ppmv, driven by enhanced CO<sub>2</sub> outgassing from volcanic activity (Jones and Jenkyns, 2001; Kidder and Worsley, 2012), have triggered OAEs (Damsté et al., 2008; Méhay et al., 2009; Bauer et al., 2016). The warmer climate during past OAEs increased weathering on land (Blättler et al., 2011; Pogge von Strandmann et  
45 al., 2013), leading to an enhanced supply of nutrients, in particular P, increasing the oceanic nutrient inventory and driving the positive feedback mentioned above. Furthermore, the enhanced release of P from sediments were suggested to maintain high levels of productivity in the Cretaceous ocean (Mort et al. 2007; Kraal et al. 2010), which would contribute to the development of OAEs. Evidence in the palaeo record indicates that the Earth had experienced several climate OAE-like states, with large-scale  
50 anoxia, euxinia and mass extinctions (Kidder and Worsley, 2010).

Could such OAEs also appear in the near future under contemporary global warming? High CO<sub>2</sub> concentrations in the atmosphere seem to be one driver for initiating OAEs and ocean deoxygenation. Projected anthropogenic CO<sub>2</sub> emissions may lead to atmospheric CO<sub>2</sub> concentrations exceeding 1000 ppmv at the beginning of the 22<sup>nd</sup> century if emissions continue to increase in a business-as-usual  
55 scenario (Meinshausen et al., 2011). Although anthropogenic CO<sub>2</sub> emissions occur over a short period compared to the long-term and relatively constant volcanic CO<sub>2</sub> emissions during OAEs (Kidder and Worsley, 2012), elevated atmospheric CO<sub>2</sub> concentrations could persist for many millennia (Clark et al., 2016). This may provide the conditions for long-term climate change and large-scale deoxygenation. There is thus some concern that anthropogenic CO<sub>2</sub> emissions could potentially trigger  
60 another OAE (Watson et al., 2017). Yet, Kidder and Worsley (2012) argue that emissions of global fossil fuel reserves are insufficient to drive a modern OAE, but may instead lead to widespread suboxia.

During climate warming, ocean productivity could switch from P to nitrogen (N) limitation (Saltzman, 2005). N limitation could arise from enhanced denitrification in a more anoxic ocean, but at the same  
65 time low N to P ratios would be expected to stimulate N<sub>2</sub>-fixation by diazotrophs (Kuypers et al., 2004). During warmer and wetter climates, however, a reduced supply of aeolian Fe may limit marine N<sub>2</sub>-fixation (Kidder and Worsley, 2010). N<sub>2</sub>-fixation in regional proximity with OMZs can lead to net N losses due to mass balance constraints (Landolfi et al., 2013), which may even reverse the net effect of N<sub>2</sub>-fixation on the nitrogen inventory.

70 Recently, Niemeyer et al. (2017) showed in a model study that P weathering and sedimentary P release in a business-as-usual CO<sub>2</sub>-emission (RCP8.5) scenario could strongly enlarge the marine P inventory and lead to a 4 to 5-fold increase in the suboxic water volume (dissolved oxygen (O<sub>2</sub>) concentrations less than 5 mmol m<sup>-3</sup>) on millennial timescales. Here, we build on this study and test the sensitivity of the marine P and O<sub>2</sub> inventories in a climate change scenario on millennial timescales to different  
75 model formulations of P weathering and benthic fluxes. We aim to provide better constraints on future ocean deoxygenation and assess the biogeochemical feedbacks triggered by P addition. In Sect. 2 we



present the experimental design and the model parameterizations of continental P weathering and of benthic P release. In Sect. 3 we assess uncertainties in P fluxes due to different assumptions about the P weathering fluxes, different model formulations of benthic P fluxes, improved representation of bathymetry and anthropogenic P fluxes. Consequences for deoxygenation and for the biogeochemical cycling of nutrients are discussed.

## 2 Model and Experimental Design

### 2.1 Model

We applied the University of Victoria (UVic) Earth System Model (ESM) version 2.9 (Weaver et al., 2001), which has been used in several studies to investigate ocean oxygen dynamics (Schmittner et al., 2007; Oschlies et al., 2008; Getzlaff et al., 2016; Keller et al., 2016; Landolfi et al., 2017). The UVic model consists of a terrestrial model based on TRIFFID and MOSES (Meissner et al., 2003), an atmospheric energy-moisture-balance model (Fanning and Weaver, 1996), a sea-ice model (Bitz and Lipscomb, 1999) and the general ocean circulation model MOM2 (Pacanowski, 1996). Horizontal resolution of all model components is  $1.8^\circ$  latitude  $\times$   $3.6^\circ$  longitude. The ocean model has 19 layers with layer thicknesses ranging from 50 m for the surface layer to 500 m in the deep ocean. The marine ecosystem was represented by a NPZD model (Keller et al., 2012). Organic matter transformations (production, grazing, degradation) were parameterized using fixed stoichiometric molar ratios (C:N:P, 106:16:1) and directly related to the production and, in oxygenated waters, utilization of  $O_2$  (O:P, 160). When  $O_2$  is depleted in the model, organic matter is respired using nitrate ( $NO_3^-$ ) (i.e. microbial denitrification). An  $O_2$  concentration of  $5 \text{ mmol m}^{-3}$  was used as switching point from aerobic respiration to denitrification. Sedimentary denitrification was not considered in this model configuration, such that water column denitrification and  $N_2$ -fixation dictate the oceanic N balance. No explicit iron cycle was simulated and iron limitation was approximated with prescribed seasonally varying dissolved iron concentrations (Keller et al., 2012). Parameterizations of benthic and weathering fluxes of P were extended from the study of Niemeyer et al. (2017). Implementations of a calcium carbonate sediment model (Archer, 1996) and a parameterization for silicate and carbonate weathering (Meissner et al., 2012) were applied in all simulations. When P weathering and anthropogenic P fluxes were applied (see Sect. 2.2), the global P flux was distributed over all river basins, in every grid box, weighted by river discharge rates.

### 2.2 Experimental Design

Twelve different model simulations were performed to explore the range of uncertainties for the long-term development of the oceanic P inventory (Table 1). Each simulation started from an Earth system state close to equilibrium under preindustrial atmospheric  $CO_2$  concentrations, prescribed wind fields and present-day orbital forcing. Spin-up runs lasting 20,000 simulation years or longer were made for each simulation to reach equilibrium. In the spin-up runs for simulations with benthic P fluxes (purple and red in Table 1), the marine P inventory was kept constant by instantaneously compensating oceanic



P loss (burial) by P weathering fluxes to the ocean. For model simulations without benthic P fluxes (black and blue in Table 1), one common spin-up run was performed without P weathering fluxes.

115 All transient simulations started in the year 1765 and ended in year 5000. Simulations were forced with anthropogenic CO<sub>2</sub> emissions (fossil fuel and land use change) according to the extended RCP 8.5 scenario until the year 2300 (Meinshausen et al., 2011), followed by a linear decline to zero CO<sub>2</sub> emissions by the year 3000. Warming from non-CO<sub>2</sub> greenhouse gases and the effect of sulphate aerosols were prescribed as radiative forcing (Eby et al., 2013). Non CO<sub>2</sub>-emission effects from land-

120 use change were not considered. The reference simulation (*Ref*) was performed without weathering and without burial fluxes of P, meaning that the P inventory of the ocean remained unchanged. The remaining transient simulations applied either variable climate-sensitive weathering anomalies (without burial) or time-variable burial fluxes (with constant weathering) to the ocean (Table 1).

### 2.3 Burial experiments

125 The water column model is not coupled to a prognostic and vertically resolved sediment model. Instead, P burial in the sediment ( $BUR_p$ ) was determined in every grid box from the difference between the simulated detritus P rain rate to the sediment ( $RR_p$ ) and the benthic release of dissolved inorganic P from the sediment ( $BEN_p$ ):

$$BUR_p = RR_p - BEN_p \quad (1)$$

where  $RR_p$  is the detritus flux from the ocean (in P units).  $BEN_p$  was calculated locally by a “transfer function”, which parameterizes sediment/water exchange of P as a function of the rain rate of organic matter and the bottom water O<sub>2</sub> concentration. Preferential P release, relative to carbon (C), is observed in sediments overlain by O<sub>2</sub>-depleted bottom waters (Ingall and Jahnke, 1994). Benthic P release was dependent on the dissolved inorganic carbon release ( $BEN_C$ ) from organic matter degradation in the sediment and the C:P regeneration ratio  $r_{C:P}$  (Wallmann, 2010; equation 2):

$$BEN_p = \frac{BEN_C}{r_{C:P}} \quad (2)$$

135  $BEN_C$  was computed (Eq. 3a) as the difference of the carbon rain rate to the sediment ( $RR_C$ ) and a ‘virtual’ organic carbon burial flux ( $BUR_C$ ). There is no explicit treatment of organic C burial in the model, and instead all organic C is remineralized in the deepest ocean layer.  $BUR_C$  is dependent on the simulated organic C rain rate and bathymetry (Flögel et al., 2011). Burial of organic C is more efficient on the shelf and continental margins (Eq. 3b) than for the deep sea (Eq. 3c, sediment below 1000m

140 water depth):

$$BEN_C = RR_C - BUR_C \quad (3a)$$

$$BUR_C = 0.14 \cdot RR_C^{1.11} \quad (3b)$$

$$BUR_C = 0.014 \cdot RR_C^{1.05} \quad (3c)$$

where  $RR_C$  is in mmol C m<sup>-2</sup> a<sup>-1</sup>.  $r_{C:P}$  (in Eq. 4) depends on the bottom water oxygen concentration and was calculated according to (Wallmann, 2010; equation 4).

$$r_{C:P} = Y_F - A \cdot \exp(-O_2/r) \quad (4)$$

where O<sub>2</sub> is in mmol m<sup>-3</sup> and the coefficients and their uncertainties are  $Y_F=123\pm24$ ;  $A=112\pm24$ ;  $r=32\pm19$  mmol m<sup>-3</sup>. Under high O<sub>2</sub> conditions  $r_{C:P}$  is 123, which is close to the Redfield ratio of 106.



145 Under low  $O_2$  conditions,  $r_{C:P}$  is lower than 106, which leads to a preferential P release from organic matter and, eventually, a net release of P from the sediment ( $BEN_P > RR_P$ , in Eq. 1).

The UVic model has a coarse standard model bathymetry with a horizontal resolution of  $1.8^\circ$  latitude x  $3.6^\circ$  longitude. This does not adequately represent continental shelves and slopes. To overcome this limitation, sinking organic matter interacts with the sediment on a detailed subgrid bathymetry (Somes et al., 2013). The subgrid bathymetry was inferred from ETOPO2v2<sup>1</sup> (National Geophysical Data Center, 2006). Fractional coverage of every ocean grid box by seafloor was calculated on each model depth level. Sinking organic matter is partially intercepted at the bottom of each grid box by a sediment layer and the intercepted amount depends linearly on the fractional coverage of the grid box by seafloor. At the seafloor, organic matter is remineralized on the subgrid bathymetry for P in accordance with Eq. (1) and Eq. (2), whereby organic C and N are completely remineralized under oxygen or nitrate utilization without any burial. The subgrid-scale parameterization leads to a better vertical representation of benthic fluxes of P and simulated sediment rain rates of detritus (see Sect. 3.2). The subgrid bathymetry does not affect other processes like circulation, advection or mixing.

Burial fluxes of P were applied in the simulations *Bur*, *Bur\_noSG*, *Bur\_Dun*, *Bur\_low*, *Bur\_high* and 160 *Bur\_res*. The default *Bur* model configuration uses Eq. (3) (Flögel et al., 2011) and the subgrid-scale bathymetry. Uncertainties in benthic P fluxes were examined by modifying this default model configuration. For the simulation *Bur\_noSG* (i.e. without subgrid-scale parameterization), P fluxes at the sediment-ocean interface were calculated using the coarser standard model bathymetry, which barely reproduce the global coverage of shelf areas (compare hypsometries in suppl. Fig. S1).

165 In the *Bur\_Dun* simulation  $BUR_C$  was calculated using Eq. (5) with  $RR_C$  in  $\text{mmol C m}^{-2} \text{d}^{-1}$ ; Dunne et al. (2007):

$$BUR_C = RR_C \cdot \left[ 0.013 + \frac{0.53 \cdot RR_C^2}{(c + RR_C)^2} \right] \quad (5)$$

Where  $c = 7 \text{ mmol C m}^{-2} \text{d}^{-1}$ . This parameterization leads to high (low) organic C burial rates for high (low) organic C rain rates. This formulation is different to the standard formulation of burial in Eq. (3b, c) where burial depends on the C rain rates and in addition on the water depth. In the standard 170 formulation, C burial is an magnitude larger in slope and shelf regions compared to the deep ocean.

We examined the sensitivity of P burial to the uncertainty of the parameters in Eq. (4) describing the carbon to phosphorus regeneration ratio  $r_{C:P}$ . Given means and standard deviations for the parameters  $Y_F=123\pm24$ ;  $A=112\pm24$ ;  $r=32\pm19$  and assuming a Gaussian distribution, 100,000 independent coefficient combinations were assembled to calculate offline a range of global P burial estimates. For 175 the offline calculation, preindustrial fields of  $O_2$  and  $RR_C$  were extracted from the simulation *Bur* with a temporal resolution fine enough to resolve seasonal variations in the data. Global P burial varied between  $0.21 \text{ TmolP a}^{-1}$  (*Bur\_low*) and  $0.60 \text{ TmolP a}^{-1}$  (*Bur\_high*) for a confidence interval of 90% (coefficients are shown in Table 1). Individual spin-ups were performed for the *Bur\_low* and *Bur\_high* simulation to check that the offline calculated P burial corresponded to the online values from the spin-up. Only minor differences between the  $O_2$  fields of the *Bur* spin-up and the spin-ups for *Bur\_low* and 180

<sup>1</sup> <https://www.ngdc.noaa.gov/mgg/global/etopo2.html>



*Bur\_high* simulations were noted (not shown), which implies negligible errors in the offline calculation of the preindustrial global P burial.

The implemented transfer functions (Eq. 2 and 4) assume unlimited local reservoirs of sedimentary P, meaning that the cumulative release of P may exceed the local inventory of P in the sediment if the benthic fluxes are sustained over a longer period of time. In the simulation *Bur\_res* we tested the impact of this simplification by applying sediment inventory restrictions to sediment P release. An upper limit sediment P inventory was calculated based on the following assumptions for the continental shelf and slope. We assume that the top 10 cm of the sediment column are mixed by organisms and are hence regarded as the active surface layer that is in contact with the overlying bottom water.

185 Considering a mean porosity of 0.8 and a mean density of dry particles of  $2.5 \text{ g cm}^{-3}$ , the mass of solids in this layer is  $5 \text{ g cm}^{-2}$  (Burwicz et al., 2011). The mean concentration of total P in continental shelf and slope sediments is 0.07 wt-% equal to  $22.6 \text{ } \mu\text{mol/g}$  (Baturin, 2007). Together, these assumptions convert to a local inventory of total solid P in the active surface layer of  $113 \text{ } \mu\text{mol cm}^{-2}$ . We assume that shelf and slope sediments can release up to 100 % of this total inventory ( $RES_p$ ) under low oxygen

195 conditions. The reservoir can be fully replenished by P supply from the water column. Any excess P is assumed to be permanently buried:

$$\Delta RES_p = RR_p - BEN_p; 0 \geq RES_p \geq 113 \text{ } \mu\text{mol/cm}^2 \quad (6)$$

Local values of  $RES_p$  adjust during the spin-up according to the environmental conditions. Our pragmatic sediment inventory approach most likely overestimates the upper limit of P that can be released from the sediments. For example, under low  $O_2$  conditions, part of the releasable or reactive P is transformed into authigenic P and permanently buried (Filippelli, 2001).

200

All *Bur* experiments applied a constant global weathering flux ( $W_{p,const}$ ) as established during the respective spin-up run (see Table 1 for values of  $W_{p,const}$  for the different *Bur* experiments).

$$W_p = W_{p,const} \quad (7)$$

## 2.4 Weathering Experiments

Uncertainties in the ocean P inventory due to weathering processes and anthropogenic fluxes of P were examined with the model simulations *Anthr*, *Weath0.05*, *Weath0.10*, *Weath0.15* and *Weath0.38*.

205

In simulations *Weath0.05*, *Weath0.10*, *Weath0.15*, *Weath0.38* the global weathering flux of P to the ocean ( $W_p$ ) was parameterized in terms of an anomaly relative to a preindustrial P weathering flux ( $W_{p,0}$ ) according to Eq. (8).

$$W_p = W_{p,0} \cdot (f(NPP, SAT) - 1). \quad (8)$$

The weathering function  $f$  is given in Eq. (9). Values of  $W_{p,0}$  are given in Table 1 and derived below.

210 The chosen anomaly approach assumes that, at steady state,  $W_{p,0}$  is balanced by a respective global burial flux and hence can be neglected during the spin-up. In these simulations no benthic P fluxes were applied and for preindustrial conditions the weathering function  $f(NPP, SAT)$  equals 1 and hence  $W_p$  equals  $0 \text{ TmolP a}^{-1}$ . The dynamic weathering function  $f$  (Eq. 9) was adopted from Niemeyer et al. (2017) and is originally based on an equation from Lenton and Britton (2006) for carbonate and silicate weathering. Following Niemeyer et al. (2017), we assumed that the release of P is proportional to the chemical weathering of silicates and carbonates on a global scale. Equation (9) describes the sensitivity

215



of terrestrial weathering to the change of global terrestrial net primary production ( $NPP$ ) and global mean surface air temperature ( $SAT$ ):

$$f = 0.25 + 0.75 \cdot (NPP/NPP_0) \cdot (1 + 0.087(SAT - SAT_0)). \quad (9)$$

with  $NPP_0$  and  $SAT_0$  being the respective preindustrial values. Increasing  $SAT$  and  $NPP$  lead to enhanced weathering. The upper estimate of  $W_{P,0}$  in *Weath0.38* was inferred from the P burial reference simulation *Bur*, assuming that the global integral of burial is compensated by the preindustrial global weathering flux (i.e. the global marine P inventory is in steady state). With the simulations *Weath0.05*, *Weath0.10*, *Weath0.15*, *Weath0.38* we explored the range of  $W_{P,0}$  estimates as derived from observational studies, which range from 0.05 to 0.30 TmolP a<sup>-1</sup> (see Fig. 1, Benitez-Nelson, 2000; Compton et al., 2000; Ruttenberg, 2003). These studies indicate that total P fluxes to the oceans are higher than interfered from dissolved inorganic P fluxes. A small amount of fluvial P is delivered to the ocean as dissolved inorganic P, but the majority (90%) is particulate (inorganic and organic) P (Compton et al., 2000). The fast transformations between dissolved and particulate P in rivers (seconds to hours) (Withers and Jarvie, 2008) suggest a much higher amount of P that is available for marine organism than derived from dissolved inorganic P concentrations. A large amount of bioavailable P in rivers is present as loosely sorbed and iron-bound P. Estimates of bioavailable P are given in Fig. 1 (Benitez-Nelson, 2000; Compton et al., 2000; Ruttenberg, 2003), which are much higher than the estimates for dissolved inorganic P (0.018 TmolP a<sup>-1</sup> from Seitzinger et al. (2005) or 0.03 TmolP a<sup>-1</sup> from Filippelli (2002)). Taking into account only fluxes of dissolved inorganic P would strongly underestimate the effect of weathering fluxes as a P source to the ocean. The weathering parametrization (Eq. 9) was used to scale preindustrial fluvial fluxes of bioavailable P that is delivered in UVic to the ocean as dissolved inorganic P. In the model, no distinction was made between particular and dissolved fluvial fluxes of P.

Uncertainties to other weathering parameterizations were not investigated in this study. Our parameterization predicts similar weathering rates to other weathering formulations (Meissner et al., 2012, their Fig. 6a). Since weathering is calculated on a global scale, we cannot study the effects of regional lithology and soil shielding on weathered P (Hartmann et al., 2014).

Finally, global anthropogenic P fluxes from fertilization, soil loss due to deforestation and sewage as projected by Filippelli (2008) were prescribed in the simulation *Anthr*.

### 245 3. Uncertainties in Phosphorus Inventory

The large range of projected global phosphorus (P) fluxes to the ocean from sediments or weathering (Fig. 2a) leads to uncertainties in future P inventories by up to 60% of the present-day value until year 5000 (Fig. 2b). All simulations show negligible differences in atmospheric CO<sub>2</sub> concentrations and hence undergo a similar climate development. Maximum CO<sub>2</sub> concentrations of 2200 ppmv were reached in year 2250 and then declined to 1100 ppmv by year 5000, comparable to results from Clark et al. (2016). We found that the large range in P fluxes was not related to differences in the climate or atmospheric CO<sub>2</sub> forcing, but rather to differences in parameterizations of P land-ocean (Sect. 3.1) and sediment-ocean (Sect. 3.2) interactions.



### 3.1. Fluvial P Fluxes: Weathering and Anthropogenic

255 Largest uncertainties in the P inventory are related to the large range of P weathering fluxes (Fig. 2,  
blue curves). Upper and lower estimates of P weathering fluxes differ by a factor of 6 (Fig. 2a, blue  
lines). In our weathering simulations, weathering anomalies depend linearly on the preindustrial  
weathering flux,  $W_{P,0}$ , estimate (see Eq. 8) because the climate development is essentially equal across  
the simulations. Therefore, the choice of  $W_{P,0}$  (Fig. 1a) is a major source of uncertainty for projected  
260 future land-ocean P fluxes.

Weathering fluxes increased from the pre-industrial value by a factor of 2.5 until year 5000 for  
atmospheric CO<sub>2</sub> concentrations of 1100 ppmv. This is comparable with the two- to four-fold increase  
in weathering fluxes estimated during OAE 2 approximately 91 Ma ago (Pogge von Strandmann et al.,  
2013) when atmospheric CO<sub>2</sub> concentrations increased to about 1000 ppmv (Damsté et al., 2008).

265 In contrast to weathering-induced P input, anthropogenic P fluxes (Filippelli, 2008) influence the  
global marine P inventory only in the near future (Fig. 2a, black dashed line). A decline in  
anthropogenic P fluxes after year 2100 is expected due to the depletion of the easily reachable  
phosphorite mining reserves (Filippelli, 2008).

### 3.2. Sediment Fluxes: Parameterizations, Subgrid Bathymetry, Sediment Reservoir

270 The release of P from the sediment is strongly dependent on the O<sub>2</sub> concentration in the water above  
the sediments (Wallmann 2003; Flögel et al. 2011). Climate warming reduces O<sub>2</sub> solubility and  
ventilation of the ocean, which decreases the global O<sub>2</sub> content (more details in Sect. 4). The general  
decrease in ocean O<sub>2</sub> content may therefore cause preferential release of P from marine sediments.  
Differences in sediment P fluxes in our simulations are related to uncertainties in the parameterization  
275 of the transfer function (Fig. 2, red lines, -0.01 to 0.22 TmolP a<sup>-1</sup> by year 5000), to different  
representations of the bathymetry (Fig. 2, purple dashed line, 0.06 (without subgrid) and 0.12 (*Bur*)  
TmolP a<sup>-1</sup>) and to the way sediment P reservoirs in the sediment are represented (Fig. 2, purple solid  
line, -0.01 (limited reservoir) and 0.12 (unlimited reservoir, *Bur*) TmolP a<sup>-1</sup>).

The global P burial of approximately 0.2 TmolP a<sup>-1</sup> (Fig. 3) (Filippelli and Delaney, 1996; Benitez-  
280 Nelson, 2000; Ruttenger, 2003) is relatively well reproduced by simulations *Bur\_low* and *Bur\_Dun*.  
The simulation with the standard UVic bathymetry (*Bur\_noSG*) underestimates P burial by 60% while  
the simulations *Bur\_high*, *Bur* and *Bur\_res* overestimate P burial by 180%, 90% and 80% with respect  
to estimates based on observations. The transient response of the P release to O<sub>2</sub> was stronger for  
simulations with low burial and vice versa (Fig. 2), except for simulation *Bur\_res*. In *Bur\_res*, a  
285 significant reduction in the transient P release occurred due to the implementation of a finite P  
reservoir, with net global P loss due to enhanced burial at the end of the simulation. In year 5000,  
global P concentrations increased in *Bur\_res* by only 0.06 mmolP m<sup>-3</sup> compared to the global mean pre-  
industrial concentration of 2.17 mmolP m<sup>-3</sup>. This is six-fold smaller than the increase of 0.36 mmolP m<sup>-3</sup>  
in simulation *Bur* with an assumed unlimited P reservoir. The small increase in the oceanic P  
290 inventory in *Bur\_res* can be explained by the reduction in P sediment inventory rather than by changes  
in the rain rate of particulate organic matter to the sediment ( $RR_C$ ). In *Bur*, a rapid increase in the  
benthic P flux appeared in areas where the water turned suboxic and thus drove a positive benthic



feedback between P release, productivity and deoxygenation. A limited supply of P from the sediment (*Bur\_Res*) dampens this feedback.

295 With a more realistic subgrid bathymetry, simulated pre-industrial  $RR_C$  increased significantly from 180 to 1040 TgC a<sup>-1</sup> on the shelf and globally from 900 to 1500 TgC a<sup>-1</sup> compared to simulations without subgrid bathymetry. Pre-industrial  $RR_C$  with subgrid bathymetry agrees better to estimates by Bohlen et al. (2012) (Table 2) and to other field data studies reporting a range from 900 to 2300 TgC a<sup>-1</sup> (Fig. 4) (Muller-Karger et al., 2005; Burdige, 2007; Dunne et al., 2007; Bohlen et al., 2012).

300 In summary, subgrid bathymetry leads to a substantial improvement of the representation of  $RR_C$  to the sediment. More realistic benthic fluxes of P could be also attained by adjusting parameters for  $r_{C,P}$  (Eq. 4) or by using the function of Dunne et al. (2007) to calculate  $BUR_C$  (Eq. 5). The implementation of a finite P reservoir in the sediment has a substantial impact on the transient development of the global P inventory on millennial time scales.

#### 305 **4. Ocean Deoxygenation and Suboxia**

Climate change influences ocean oxygen content by changes in circulation, ocean temperature and the degradation of organic matter. In warming surface waters, the solubility of O<sub>2</sub> decreases along with an increase in stratification, which together cause the deeper ocean to become less ventilated (Bopp et al., 2002; Oschlies et al., 2018). Changes in export production and the degradation of organic matter in the ocean interior also affects O<sub>2</sub> content. In the following, we analyze the impact of different ocean P inventories on ocean deoxygenation and suboxia (Fig. 5). For a more detailed analysis we compare *Weath0.15* to the *Ref* simulation. In the *Weath0.15* simulation, the assumed preindustrial weathering flux compares well to estimates from observations (Fig. 1).

In the *Ref* simulation, global suboxic volume increased due to climate change from 0.3 to 1% until year 315 5000 and the suboxic sediment area increased from 0.06 to 0.23% (Fig. 5, black line). In the *Weath0.15* simulation, the increase in suboxic volume (suboxic sediment area) was more than 2 (3) times higher than for the *Ref* simulation. The expansion of suboxic sediment areas was also enhanced for simulations with benthic fluxes, which could be related to regional feedbacks between increasing marine productivity, decreasing oxygen and enhanced sedimentary P release (Tsandev and Slomp, 2009). The explicitly simulated finite sedimentary P reservoir in simulation *Bur\_res* places an upper limit to the benthic release of P and dampens these regional feedbacks, resulting in a weaker spreading of suboxic waters by only 17% compared to the *Ref* simulation.

In the following sections, we show how the expansion of suboxia is related to net primary production in the ocean (NPP), the export of organic matter (Sect. 4.1) and to nitrogen limitation (Sect. 4.2). 325 Finally, we show how changes in O<sub>2</sub> solubility and utilization vary over time and affect the global O<sub>2</sub> inventory (Sect. 4.3). The latter approach gives another perspective because changes in O<sub>2</sub> inventories are a global integrated signal in comparison to the extent of suboxia, which are consequence of more local processes.



#### 4.1. Enhanced Biological Pump

330 The biological carbon pump can be summarized as the supply of biologically sequestered CO<sub>2</sub> to the  
deep ocean. In the euphotic zone phytoplankton and diazotrophs take up CO<sub>2</sub>, a process that is  
intensified by elevated PO<sub>4</sub> concentrations in the surface ocean (Fig. 6a). Part of the organic matter  
sinks out of the euphotic zone (Fig. 6b) to the ocean interior, where it is respired using O<sub>2</sub>. It is  
therefore P supply to the surface waters that explains the differences in deoxygenation between the  
335 simulations. Circulation changes could also affect the supply of O<sub>2</sub> to the ocean interior. However, no  
significant differences in climate and circulation appeared among the simulations and therefore the  
global-warming induced circulation changes affected all simulations in the same way.

In the *Ref* simulation, net primary production (NPP, Fig. 6a black line) increased from 45 to 70 TmolP  
a<sup>-1</sup> (57 to 89 GtC a<sup>-1</sup>) by the end of the simulation. In *Weath0.15*, enhanced P supply to the ocean led to  
340 a doubling of NPP compared to the *Ref* simulation. The P inventory increased continuously, but NPP  
did not follow this trend and instead peaked in year 4000. In year 5000, all simulations, excluding  
*Weath0.38*, showed a similar response of NPP to the P addition with an increase in NPP of 19 TmolP a<sup>-1</sup>  
(relative to the *Ref* simulation) per 10% increase in P inventory. In *Weath0.38* the response was  
weaker and NPP increased by 8 TmolP a<sup>-1</sup> per 10% rise in the P concentration. P is less effectively  
345 utilized in simulations with large oceanic P inventories. Higher ocean temperatures enhanced  
remineralization of organic matter in the shallower ocean so that the overall export to NPP ratio  
decreased from its preindustrial value of 0.12 to an average value among all simulations of 0.08 by year  
5000. To summarize, NPP and export of organic matter is sensitive to P addition. However, the  
proposed positive feedback between P, NPP, export of organic matter, and deoxygenation was limited  
350 in our simulations due to a negative feedback related to nitrate availability. This is showed and  
explored in the following section.

#### 4.2. Nitrogen Limitation

At the end of the spin-up the N sink by denitrification and the N source by N<sub>2</sub>-fixation were balanced.  
In the *Ref* simulation, climate warming enlarged the oxygen minimum zones, which enhanced  
355 denitrification in the tropics (not shown). In all simulations, N<sub>2</sub>-fixation was stimulated by the addition  
of P to the ocean and was sensitive to rapid changes in the supply of P (compare Fig. 7a and Fig 2a).  
However, N<sub>2</sub>-fixation by diazotrophs (Fig. 7a) was not able to balance the loss by denitrification  
because low temperatures in polar regions and iron limitation at lower latitudes inhibit growth of  
diazotrophs (Fig. S2), leading to a substantial amount of excess phosphate in the surface waters of  
these regions (Fig. S3). As a consequence, nitrate decreased globally by 4 mmolN m<sup>-3</sup> until year 5000  
360 (Fig. 7b). In low-N and high-P environments, diazotrophs have a competitive advantage over other  
phytoplankton. In the simulations with P supply, N<sub>2</sub>-fixation by diazotrophs was stimulated (Fig. 7a)  
and partly counteracted the nitrate loss by denitrification. The loss in nitrate led to a decrease in  
globally averaged N to P ratios. In the *Ref* simulation, N:P decreased from 14 to 12 and for the  
365 *Weath0.15* simulation it decreased to 10, which contributed further to a N limiting ocean. The nitrogen  
cycle was not able to recover from the decrease in N:P ratio with respect to pre-industrial values. In the  
model, phytoplankton biomass assumed to grow with fixed Redfield stoichiometry. The ability of



370 phytoplankton to adapt to changing N:P ratios was not considered. Phytoplankton organisms may  
utilize the excess in P if they are able to adapt their stoichiometry to the decreasing N:P ratios, which  
could then lead to an increase marine biological productivity and greater deoxygenation.

#### 4.3. Temporal Variations of Deoxygenation

375 Anomalies in circulation, ocean temperature and remineralisation of organic matter affect oceanic O<sub>2</sub>  
levels in a climate-warming scenario. In the *Ref* simulation, the O<sub>2</sub> inventory (Fig. 8a) decreased by 60  
Pmol O<sub>2</sub> by the year 3000 and then recovered by year 5000. In *Weath0.15*, weathered P enhanced  
deoxygenation and led to a greater decrease in O<sub>2</sub> than in the *Ref* simulation. The O<sub>2</sub> decrease was up to  
70 Pmol in year 3300 and O<sub>2</sub> still showed a negative anomaly of 24 Pmol O<sub>2</sub> by the year 5000. Global  
anomalies in oxygen were due to changes of the Apparent Oxygen Utilization (AOU, Fig. 8b) and the  
O<sub>2</sub> saturation level (Fig. 8c). Changes in O<sub>2</sub> saturation were similar across the model simulations and  
followed with a delay surface ocean temperature. The circulation and ventilation of the ocean were  
380 similar in the model simulations because differences in surface temperatures were negligible and the  
atmospheric forcing of the ocean circulation was identical. So that differences in AOU depended  
almost only on biological O<sub>2</sub> consumption and AOU anomalies were directly yet inversely related to  
the changes in O<sub>2</sub> levels. Hence, biological consumption explained variations in O<sub>2</sub> content among the  
different model simulations (compare Fig. 8a and 8b). Increasing O<sub>2</sub> utilization contributed to the  
385 decrease of the O<sub>2</sub> until year 3000. Thereafter, a distinct negative trend in AOU with a similar slope  
was observed among all simulations and contributed to a re-oxygenation of the ocean. For simulations  
with larger P inventories, the AOU had a larger positive offset to the *Ref* simulation.

390 In a model with constant stoichiometry for elemental exchange by biological processes, anomalies in  
AOU (Fig. 9, blue lines) can be explained by the difference between total integrated nutrients (Fig. 9,  
red and black solid lines as anomalies) and preformed nutrients (Fig. 9, red and black dashed lines as  
anomalies). Preformed nutrients correspond to the fraction that leaves the surface ocean unutilized by  
phytoplankton. For example in the Southern Ocean, a large fraction of nutrients leaves the surface as  
preformed nutrients. The fraction of utilized and preformed nutrients can change during a transient  
simulation and could affect the oxygen state of the ocean.

395 In the *Ref* simulation (Fig. 9a), the anomaly of preformed dissolved inorganic P was directly inverse to  
the anomaly of AOU because the oceanic P Inventory was conserved in this simulation. Until year  
2200, changes in circulation and climate are likely the main cause for the reduction in preformed N and  
P in the *Ref* simulation since global N and P inventories were constant (Fig 9a, solid red and black  
line). During continuous and intense ocean warming, a weakening of the meridional overturning (not  
400 shown) reduced ocean ventilation. The meridional overturning decreased from 17 Sv (pre-industrial) to  
11 Sv in year 2200. The continuous warming and stratification of the ocean reduces the supply of  
nutrients to the surface layer from the deep ocean. This is consistent with a reduction of the export of  
organic matter until year 2200 (Fig. 6b). The balance between exported P out of the surface ocean and  
supplied P controls changes in AOU. We speculate that a weaker overturning increased the residence  
405 time of water and nutrients in the surface ocean. Nutrients staying longer in the euphotic zone are with



a higher probability biologically consumed. This implies more efficient utilization of nutrients and, hence, the reduction in preformed nutrients and an increase in AOU.

Enhanced suboxia after year 2200 drove excess denitrification and a decline in nitrate (Fig. 9a red solid line) in the *Ref* simulation. The decline in nitrate could explain the negative trend in AOU anomalies (Fig. 9a blue solid line) and therefore a negative feedback on the global deoxygenation. In year 2200, overturning had started to recover quickly and increased to 21 Sv in year 3000 (+24% relative to preindustrial values), which drove a faster overturning of organic matter in the surface ocean and a decrease in global AOU. We assume that the slight increase in export by 5% (relative to preindustrial values) was not strong enough to compensate for the by +24% faster overturning, which reduced the residence time of nutrients in the surface ocean.

P addition in the *Weath0.15* simulation stimulated N<sub>2</sub>-fixation by diazotrophs and counteracted N-loss by denitrification (Fig. 9b, red solid line). This led to an increase in N inventory by 17 Pmol O<sub>2</sub>-equivalents compared to the *Ref* simulation. Furthermore, the high availability of P seems to reduce preformed N by 6 Pmol O<sub>2</sub> equivalents. Both explain the difference in AOU between *Weath0.15* and *Ref* of 24 Pmol O<sub>2</sub> at the end of the simulation (Fig. 8b). However, denitrification still exceeded N<sub>2</sub>-fixation, which led to low levels of nitrate. From year 5000 approximately all of the added P in the *Weath0.15* simulation remained unused by phytoplankton, left at the surface ocean as preformed P and was afterwards stored in the deep ocean. Phytoplankton was not able to utilize the excess P because it was limited in nitrate. Diazotrophs were not able to compensate for the lack in N due to iron limitation and low surface temperatures in the polar oceans. The denitrification feedback driven by the spread of suboxic conditions in the tropics had reduced further N availability for the phytoplankton and reduced the effect of P addition on the global oxygen level.

## 5. Discussion and Conclusions

The P inventory is very sensitive to the weathering and benthic flux parameterizations tested in our model. Large uncertainties (Fig. 2, blue lines) derive from poorly constrained estimate for the preindustrial P weathering flux that ranges from 0.05 to 0.30 Tmol P a<sup>-1</sup> (Benitez-Nelson, 2000; Compton et al., 2000; Ruttenger, 2003). The preindustrial weathering flux in simulation *Weath0.15* (0.15 Tmol P a<sup>-1</sup>) is well in this range. In this simulation, enhanced weathering leads to an increase in the global ocean P inventory by 25% until year 5000 (Fig. 2, blue dotted line). Benthic fluxes of P were simulated using transfer functions on a subgrid bathymetry. Applying the transfer functions without taking into account the local sedimentary P inventory can greatly overestimate the release of benthic P on long time scales. In the UVic model, the application of finite benthic P inventories limited the benthic release significantly. Under low-oxygen conditions, sediments were P depleted already after a few years to decades. In our simulation, this resulted in an increase in the global oceanic P inventory by just 3% (Fig. 2, magenta solid line). This implies that benthic release of P is actually negligible in comparison to the weathering fluxes of P, but the UVic model does not resolve coastal processes such as the deposition of reactive particulate P from rivers on the continental shelves and its dissolution and release to the water column. A more detailed representation of coastal processes would be necessary to simulate burial and release of fluvial P. Further, we find that a more realistic bathymetry substantially



445 improves the simulated rain rate of particular organic carbon to the sediment (Table 2), particularly on  
the shelf, which most models do not resolve. Anthropogenic P fluxes increased the global P inventory  
by just 2% (Fig. 2, black dashed line). In summary, our best estimate for changes in the total global  
ocean P inventory by the year 5000 amounts to +30%, which was dominated by weathering. This  
seems to be surprisingly high, but several studies indicate that changes in past climate could also have  
450 been accompanied with substantial changes in the P inventory but at a much lower pace (Planavsky et  
al., 2010; Monteiro et al., 2012; Wallmann, 2014).

The increased P inventory (Fig. 2b) promotes deoxygenation (Fig. 5) and expansion of suboxia, but it  
also causes a net loss of nitrate, which appears to further limit the full utilization of P by phytoplankton  
in our simulations. Wallmann (2003), using a box model, already recognized that for a eutrophic ocean,  
455 nitrate might ultimately limit marine productivity. As a consequence, large amounts of P leave the  
surface ocean as preformed P (Fig. 9b) with no further impact on O<sub>2</sub> levels in the ocean interior. Low  
N/P ratios are thought to give N<sub>2</sub>-fixers a competitive advantage over ordinary phytoplankton and lead  
to an increase in N<sub>2</sub>-fixation (Fig. 7a). A substantial increase in N<sub>2</sub>-fixation was also inferred from a  
palaeo study of sedimentary nitrogen isotopes by Kuypers et al. (2004). However, high denitrification  
460 rates remove nitrate from the global ocean and in the UVic model N<sub>2</sub>-fixers are not able to compensate  
for this loss (Fig. 7b) because low temperatures in polar regions and iron limitation at lower latitudes  
inhibit growth of diazotrophs (Fig. S2) and a substantial amount of excess phosphate remains in the  
surface waters in these regions (Fig. S3). General circulation models without a N cycle, or box models  
without realistic representation of habitats suitable for N<sub>2</sub>-fixers, would miss this important negative  
465 feedback limiting global deoxygenation.

Some additional model limitations are a cause for uncertainty in our results. We considered a fixed  
Redfield-ratio stoichiometry. In future deoxygenation studies, an optimality-based model for nutrient  
uptake with variable nutrient ratios (Pahlow et al., 2013) could be applied to investigate how well  
marine organisms adapt to a changing nutrient availability in the global ocean. Sea level change and the  
470 implied bathymetry change were not simulated in the UVic model. In future projections, higher surface  
air temperatures would lead to a rise in sea level, which increase global coverage of shelf areas. Burial  
of P is more effective on the shelf (Flögel et al., 2011), which would remove P from the ocean and lead  
to a lower marine P residence time (Bjerrum et al., 2006).

To conclude, climate warming leads to a larger oceanic P inventory mainly due to addition of P by  
475 weathering, but also due to the release of P from the sediment and due to anthropogenic fluxes. A  
realistic representation of shelf bathymetry improves the predicted benthic P fluxes. Transfer functions  
for benthic P release should consider the sedimentary P inventory. However, the largest uncertainties in  
the projection of oceanic P inventory are due to poorly constrained weathering fluxes of P. Although  
additional deoxygenation is driven by P addition to the ocean, the degree of deoxygenation – and hence  
480 the positive redox-related feedback on benthic P fluxes is eventually limited by the availability of N  
and the apparent inability of the modelled N<sub>2</sub> fixation to respond to the larger P inventory.

**Acknowledgements.** This work is a contribution to the Sonderforschungsbereich (SFB) 754  
“Climate-Biogeochemical Interactions in the Tropical Ocean”.



485

**Data and Code Availability.** The model data and the model code are available at [https://data.geomar.de/thredds/catalog/open\\_access/kemena\\_et\\_al\\_2018\\_esd/catalog.html](https://data.geomar.de/thredds/catalog/open_access/kemena_et_al_2018_esd/catalog.html).

490 **Author contributions.** All authors discussed the results and wrote the manuscript. T.P.k. led the writing of the manuscript and the data analysis.

**Competing interests.** The authors declare that they have no conflict of interest.

**Bibliography:**

- 495 Archer, D.: A data driven model of the global calcite lysocline, *Global Biogeochem. Cycles*, 10, 511–526, doi: 10.1029/96GB01521, 1996.
- Baturin, G. N.: Issue of the relationship between primary productivity of organic carbon in ocean and phosphate accumulation (Holocene-Late Jurassic). *Lithol. Miner. Resour.*, 42, 318–348, doi: 10.1134/S0024490207040025, 2007.
- 500 Bauer, K. W., Zeebe, R. E., and Wortmann, U. G.: Quantifying the volcanic emissions which triggered Oceanic Anoxic Event 1a and their effect on ocean acidification, *Sedimentology*, 64, 204–214, doi: 10.1111/sed.12335, 2017.
- Benitez-Nelson, C. R.: The biogeochemical cycling of phosphorus in marine systems, *Earth. Sci. Rev.*, 51, 109–135, doi: 10.1016/S0012-8252(00)00018-0, 2000.
- 505 Bitz, C. M., and Lipscomb, W. H.: An energy-conserving thermodynamic model of sea ice, *J. Geophys. Res.*, 104, 15669, doi: 10.1029/1999JC900100, 1999.
- Bjerrum, C. J., Bendtsen, J., and Legarth, J. J. F.: Modeling organic carbon burial during sea level rise with reference to the Cretaceous, *Geochem. Geophys. Geosyst.*, 7, Q05008, doi: 10.1029/2005GC001032, 2006.
- 510 Blättler, C. L., Jenkyns, H. C., Reynard, L. M., and Henderson, G. M.: Significant increases in global weathering during Oceanic Anoxic Events 1a and 2 indicated by calcium isotopes, *Earth Planet Sci. Lett.*, 309, 77–88, doi: 10.1016/j.epsl.2011.06.029, 2011.
- Bohlen, L., Dale, A. W., and Wallmann, K.: Simple transfer functions for calculating benthic fixed nitrogen losses and C:N:P regeneration ratios in global biogeochemical models. *Global Biogeochem. Cycles*, 26, GB3029, doi: 10.1029/2011GB004198, 2012.
- 515 Bopp, L., Le Quéré, C., Heimann, M., Manning, A. C., Monfray, P.: Climate-induced oceanic oxygen fluxes: Implications for the contemporary carbon budget, *Global Biogeochem. Cycles*, 16, 6-1-6-13, doi: 10.1029/2001GB001445, 2002.
- Burdige, D. J.: Preservation of organic matter in marine sediments: Controls, mechanisms, and an imbalance in sediment organic carbon budgets? *Chem. Rev.*, 107, 467–485, doi: 10.1021/cr050347q, 2007.
- 520 Burwicz, E. B., Rüpke, L. H., and Wallmann, K.: Estimation of the global amount of submarine gas hydrates formed via microbial methane formation based on numerical reaction-transport modeling and a novel parameterization of Holocene sedimentation. *Geochim. Cosmochim. Acta.*, 75, 4562–4576, doi: 10.1016/j.gca.2011.05.029, 2011.
- 525 Clark, P. U., Shakun, J. D., Marcott, S. A., Mix, A. C., Eby, M., Kulp, S., Levermann, A., Milne, G. A., Pfister, P. L., Santer, B. D., Schrag, D. P., Solomon, S., Stocker, T. F., Strauss, B. H., Weaver, A. J., Winkelmann, R., Archer, D., Bard, E., Goldner, A., Lambeck, K., Pierrehumbert, R. T., and Plattner, G.-K.: Consequences of twenty-first-century policy for multi-millennial climate and sea-level change, *Nat. Clim. Chang.*, 6, 360–369, doi: 10.1038/nclimate2923, 2016.
- 530 Compton, J., Mallinson, D., Glenn, C. R., Filippelli, G., Föllmi, K., Shields, G., and Zanin, Y.: Variations in the global phosphorus cycle, *Marine Authigenesis: From Global to Microbial*, edited by: Glenn, C. R., Prévôt, L., and Lucas, J., *SEPM Spec. Publ.*, 66, 21–33, doi:



- 10.2110/pec.00.66.0021, 2000
- 535 Damsté, J. S. S., Kuypers, M. M. M., Pancost, R. D., and Schouten, S.: The carbon isotopic response of algae, (cyano)bacteria, archaea and higher plants to the late Cenomanian perturbation of the global carbon cycle: Insights from biomarkers in black shales from the Cape Verde Basin (DSDP Site 367), *Org. Geochem.*, 39, 1703–1718, doi: 10.1016/j.orggeochem.2008.01.012, 2008.
- Dunne, J. P., Sarmiento, J. L., and Gnanadesikan, A.: A synthesis of global particle export from the surface ocean and cycling through the ocean interior and on the seafloor, *Global Biogeochem. Cycles*, 21, 1–16, doi: 10.1029/2006GB002907, 2007.
- 540 Eby, M., Weaver, A. J., Alexander, K., Zickfeld, K., Abe-Ouchi, A., Cimadoribus, A. A., Crespin, E., Drijfhout, S. S., Edwards, N. R., Eliseev, A. V., Feulner, G., Fichefet, T., Forest, C. E., Goosse, H., Holden, P. B., Joos, F., Kawamiya, M., Kicklighter, D., Kienert, H., Matsumoto, K., Mokhov, I. I., Monier, E., Olsen, S. M., Pedersen, J. O. P., Perrette, M., Philippon-Berthier, G., Ridgwell, A., Schlosser, A., Schneider von Deimling, T., Shaffer, G., Smith, R. S., Spahni, R., Sokolov, A. P., Steinacher, M., Tachiiri, K., Tokos, K., Yoshimori, M., Zeng, N., and Zhao, F.: Historical and idealized climate model experiments: an intercomparison of Earth system models of intermediate complexity, *Clim. Past*, 9, 1111–1140, doi: 10.5194/cp-9-1111-2013, 2013.
- 545 Fanning, A. F., and Weaver, A. J.: An atmospheric energy-moisture balance model: Climatology, interpentadal climate change, and coupling to an ocean general circulation model, *J. Geophys. Res.*, 101, 15111, doi: 10.1029/96JD01017, 1996.
- Filippelli, G. M.: Carbon and phosphorus cycling in anoxic sediments of the Saanich Inlet, British Columbia, *Mar. Geol.*, 174, 307–321, doi: 10.1016/S0025-3227(00)00157-2, 2001.
- 555 Filippelli, G. M.: The Global Phosphorus Cycle, *Rev. Mineral. Geochemistry*, 48, 391–425, doi: 10.2138/rmg.2002.48.10, 2002.
- Filippelli, G. M.: The Global Phosphorus Cycle: Past, Present, and Future, *Elements*, 4, 89–95, doi: 10.2113/GSELEMENTS.4.2.89, 2008.
- Filippelli, G. M., and Delaney, M. L.: Phosphorus geochemistry of equatorial Pacific sediments, *Geochim. Cosmochim. Acta.*, 60, 1479–1495, doi: 10.1016/0016-7037(96)00042-7, 1996.
- 560 Flögel, S., Wallmann, K., Poulsen, C. J., Zhou, J., Oschlies, A., Voigt, S., and Kuhnt, W.: Simulating the biogeochemical effects of volcanic CO<sub>2</sub> degassing on the oxygen-state of the deep ocean during the Cenomanian/Turonian Anoxic Event (OAE2), *Earth Planet Sci. Lett.*, 305, 371–384, doi: 10.1016/j.epsl.2011.03.018, 2011.
- 565 Getzlaff, J., Dietze, H., and Oschlies, A.: Simulated effects of southern hemispheric wind changes on the Pacific oxygen minimum zone, *Geophys. Res. Lett.*, 43, 728–734, doi: 10.1002/2015GL066841, 2016.
- Hartmann, J., Moosdorf, N., Lauerwald, R., Hinderer, M., and West, A. J.: Global chemical weathering and associated P-release - The role of lithology, temperature and soil properties, *Chem. Geol.*, 363, 145–163, doi: 10.1016/j.chemgeo.2013.10.025, 2014.
- 570 Ingall, E., and Jahnke, R.: Evidence for enhanced phosphorus regeneration from marine sediments overlain by oxygen depleted waters, *Geochim. Cosmochim. Acta.*, 58, 2571–2575, doi: 10.1016/0016-7037(94)90033-7, 1994.



- 575 Jones CE, Jenkyns HC (2001) Seawater strontium isotopes, oceanic anoxic events, and seafloor  
hydrothermal activity in the Jurassic and Cretaceous. *Am J Sci* 301:112–149. doi:  
10.2475/ajs.301.2.112
- Keller, D. P., Oschlies, A., and Eby, M.: A new marine ecosystem model for the University of Victoria  
Earth System Climate Model, *Geosci. Model Dev.*, 5, 1195–1220, doi: 10.5194/gmd-5-1195-  
2012, 2012.
- 580 Keller, D. P., Kriest, I., Koeve, W., and Oschlies, A.: Southern Ocean biological impacts on global  
ocean oxygen, *Geophys. Res. Lett.*, 43, 6469–6477, doi: 10.1002/2016GL069630, 2016.
- Kidder, D. L., and Worsley, T. R.: Phanerozoic Large Igneous Provinces (LIPs), HEATT (Haline  
Euxinic Acidic Thermal Transgression) episodes, and mass extinctions, *Palaeogeogr.  
Palaeoclimatol. Palaeoecol.*, 295, 162–191, doi: 10.1016/j.palaeo.2010.05.036, 2010.
- 585 Kidder, D. L., and Worsley, T. R.: A human-induced hothouse climate?, *GSA Today*, 22, 4–11, doi:  
10.1130/G131A.1, 2012.
- Kraal, P., Slomp, C. P., Forster, A., and Kuypers, M. M. M.: Phosphorus cycling from the margin to  
abyssal depths in the proto-Atlantic during oceanic anoxic event 2, *Palaeogeogr. Palaeoclimatol.  
Palaeoecol.*, 295, 42–54, doi: 10.1016/j.palaeo.2010.05.014, 2010.
- 590 Kuypers, M. M. M., van Breugel, Y., Schouten, S., Erba, E., and Damsté, J. S. S.: N<sub>2</sub>-fixing  
cyanobacteria supplied nutrient N for Cretaceous oceanic anoxic events, *Geology*, 32, 853–856,  
doi: 10.1130/G20458.1, 2004.
- Landolfi, A., Dietze, H., Koeve, W., and Oschlies, A.: Overlooked runaway feedback in the marine  
nitrogen cycle: The vicious cycle, *Biogeosciences*, 10, 1351–1363, doi: 10.5194/bg-10-1351-  
595 2013, 2013.
- Landolfi, A., Somes, C. J., Koeve, W., Zamora, L. M., and Oschlies, A.: Oceanic nitrogen cycling and  
N<sub>2</sub>O flux perturbations in the Anthropocene, *Global Biogeochem. Cycles*, 31, 1–20. doi:  
10.1002/2017GB005633, 2017.
- Lenton, T. M., and Britton, C.: Enhanced carbonate and silicate weathering accelerates recovery from  
600 fossil fuel CO<sub>2</sub> perturbations, *Global Biogeochem. Cycles*, 20, 1–12, doi:  
10.1029/2005GB002678, 2006.
- Méhay, S., Keller, C. E., Bermasconi, S. M., Weissert, H., Erba, E., Bottini, C., and Hochuli, P. A.: A  
volcanic CO<sub>2</sub> pulse triggered the Cretaceous oceanic Anoxic event 1a and a biocalcification  
crisis, *Geology*, 37, 819–822, doi: 10.1130/G30100A.1, 2009.
- 605 Meinshausen, M., Smith, S. J., Calvin, K., Daniel, J. S., Kainuma, M. L. T., Lamarque, J., Matsumoto,  
K., Montzka, S. A., Raper, S. C. B., Riahi, K., Thomson, A., Velders, G. J. M., and van Vuuren,  
D. P. P.: The RCP greenhouse gas concentrations and their extensions from 1765 to 2300, *Clim.  
Change*, 109, 213–241, doi: 10.1007/s10584-011-0156-z, 2011.
- Meissner, K. J., Weaver, A. J., Matthews, H. D., and Cox, P. M.: The role of land surface dynamics in  
610 glacial inception: a study with the UVic Earth System Model, *Clim. Dyn.*, 21, 515–537, doi:  
10.1007/s00382-003-0352-2, 2003.
- Meissner, K. J., McNeil, B. I., Eby, M., and Wiebe, E. C.: The importance of the terrestrial weathering  
feedback for multimillennial coral reef habitat recovery, *Global Biogeochem. Cycles*, 26, 1–20,



- doi: 10.1029/2011GB004098, 2012.
- 615 Monteiro, F. M., Pancost, R. D., Ridgwell, A., and Donnadieu, Y.: Nutrients as the dominant control on the spread of anoxia and euxinia across the Cenomanian-Turonian oceanic anoxic event (OAE2): Model-data comparison, *Paleoceanography*, 27, 1–17, doi: 10.1029/2012PA002351, 2012.
- Mort, H. P., Adatte, T., Föllmi, K. B., Keller, G., Steinmann, P., Matera, V., Berner, Z., and Stüben, D.: Phosphorus and the roles of productivity and nutrient recycling during oceanic anoxic event 2, 620 *Geology*, 35, 483–486, doi: 10.1130/G23475A.1, 2007.
- Muller-Karger, F. E., Varela, R., Thunell, R., Luerssen, R., Hu, C., and Walsh, J. J.: The importance of continental margins in the global carbon cycle, *Geophys. Res. Lett.*, 32, 1–4, doi: 10.1029/2004GL021346, 2005.
- National Geophysical Data Center, . 2-minute Gridded Global Relief Data (ETOPO2) v2, National 625 Geophysical Data Center, NOAA, doi:10.7289/V5J1012Q, 2006.
- Nickelsen, L., Keller, D. P., and Oeschies, A.: A dynamic marine iron cycle module coupled to the University of Victoria Earth System Model: The Kiel Marine Biogeochemical Model 2 for UVic 2.9, *Geosci. Model Dev.*, 8, 1357–1381, doi: 10.5194/gmd-8-1357-2015, 2015.
- Niemeyer, D., Kemena, T. P., Meissner, K. J., and Oeschies, A.: A model study of warming-induced 630 phosphorus–oxygen feedbacks in open-ocean oxygen minimum zones on millennial timescales, *Earth Syst. Dyn.*, 8, 357–367, doi: 10.5194/esd-8-357-2017, 2017.
- Oeschies, A., Schulz, K. G., Riebesell, U., and Schmittner, A.: Simulated 21st century’s increase in oceanic suboxia by CO<sub>2</sub>-enhanced biotic carbon export, *Global Biogeochem. Cycles*, 22, 1–10, doi: 10.1029/2007GB003147, 2008.
- 635 Oeschies, A., Brandt, P., Stramma, L., and Schmidtko, S.: Drivers and mechanisms of ocean deoxygenation, *Nat. Geosci.*, 11, 467–473, doi: 10.1038/s41561-018-0152-2, 2018.
- Pacanowski, R. C.: MOM2: Documentation, User’s Guide and Reference Manual, GFDL Ocean Tech. Rep. 3.2, 1996.
- Pahlow, M., Dietze, H., and Oeschies, A.: Optimality-based model of phytoplankton growth and 640 diazotrophy, *Mar. Ecol. Prog. Ser.*, 489, 1–16, doi: 10.3354/meps10449, 2013.
- Palastanga, V., Slomp, C. P., and Heinze, C.: Long-term controls on ocean phosphorus and oxygen in a global biogeochemical model, *Global Biogeochem. Cycles*, 25, 1–19, doi: 10.1029/2010GB003827, 2011.
- Planavsky, N. J., Rouxel, O. J., Bekker, A., Lalonde, S. V., Konhauser, K. O., Reinhard, C. T., and 645 Lyons, T. W.: The evolution of the marine phosphate reservoir, *Nature*, 467, 1088–1090, doi: 10.1038/nature09485, 2010.
- Pogge von Strandmann, P. A. E., Jenkyns, H. C., and Woodfine, R. G.: Lithium isotope evidence for enhanced weathering during Oceanic Anoxic Event 2, *Nat. Geosci.*, 6, 668–672, doi: 10.1038/ngeo1875, 2013.
- 650 Ruttenger, K. C.: The Global Phosphorus Cycle. *Treatise on Geochemistry*, edited by: Schlesinger, W., Elsevier, 585–643, doi: 10.1016/B0-08-043751-6/08153-6, 2003.
- Ruvalcaba Baroni, I., Topper, R. P. M., Van Helmond, N. A. G. M., Brinkhuis, H., and Slomp C. P.: Biogeochemistry of the North Atlantic during oceanic anoxic event 2: Role of changes in ocean



- circulation and phosphorus input, *Biogeosciences*, 11, 977–993, doi: 10.5194/bg-11-977-2014,  
655 2014.
- Saltzman, M. R.: Phosphorus, nitrogen, and the redox evolution of the Paleozoic oceans, *Geology*, 33,  
573–576, doi: 10.1130/G21535.1, 2005.
- Schmittner, A., Galbraith, E. D., Hostetler, S. W., Pedersen, T. F., and Zhang, R.: Large fluctuations of  
dissolved oxygen in the Indian and Pacific oceans during Dansgaard-Oeschger oscillations  
660 caused by variations of North Atlantic Deep Water subduction, *Paleoceanography*, 22, 1–17, doi:  
10.1029/2006PA001384, 2007.
- Seitzinger, S. P., Harrison, J. A., Dumont, E., Beusen, A. H. W., and Bouwman, A. F.: Sources and  
delivery of carbon, nitrogen, and phosphorus to the coastal zone: An overview of Global Nutrient  
Export from Watersheds (NEWS) models and their application, *Global Biogeochem. Cycles*, 19,  
665 1–11, doi: 10.1029/2005GB002606, 2005.
- Seitzinger, S. P., Mayorga, E., Bouwman, A. F., Kroeze, C., Beusen, A. H. W., Billen, G., Van Drecht,  
G., Dumont, E., Fekete, B. M., Garnier, J., and Harrison, J. A.: Global river nutrient export: A  
scenario analysis of past and future trends, *Global Biogeochem. Cycles*, 24, 1–16, doi:  
10.1029/2009GB003587, 2010.
- 670 Somes, C. J., Oschlies, A., and Schmittner, A.: Isotopic constraints on the pre-industrial oceanic  
nitrogen budget, *Biogeosciences*, 10, 5889–5910, doi: 10.5194/bg-10-5889-2013, 2013.
- Tsandeov, I., and Slomp, C. P.: Modeling phosphorus cycling and carbon burial during Cretaceous  
Oceanic Anoxic Events, *Earth Planet. Sci. Lett.*, 286, 71–79, doi: 10.1016/j.epsl.2009.06.016,  
2009.
- 675 Tyrrell T.: The relative influences of nitrogen and phosphorus on oceanic primary production, *Nature*,  
400, 525–531, doi: 10.1038/22941, 1999.
- Van Cappellen, P., and Ingall, E. D.: Benthic phosphorous regeneration, net primary production, and  
ocean anoxia: a model of the couple biogeochemical cycles of carbon and phosphorous,  
*Paleoceanography*, 9, 667–692, doi: 10.1029/94PA01455, 1994.
- 680 Wallmann, K.: Feedbacks between oceanic redox states and marine productivity: A model perspective  
focused on benthic phosphorus cycling, *Global Biogeochem. Cycles*, 17, doi:  
10.1029/2002GB001968, 2003.
- Wallmann, K.: Phosphorus imbalance in the global ocean?, *Global Biogeochem. Cycles*, 24, 1–12, doi:  
10.1029/2009GB003643, 2010.
- 685 Wallmann, K.: Is late Quaternary climate change governed by self-sustained oscillations in  
atmospheric CO<sub>2</sub>, *Geochim. Cosmochim. Acta.*, 132, 413–439, doi: 10.1016/j.gca.2013.10.046,  
2014.
- Watson, A. J., Lenton, T. M., and Mills, B. J. W.: Ocean deoxygenation, the global phosphorus cycle  
and the possibility of human-caused large-scale ocean anoxia, *Philos. Trans. R. Soc. A Math.*  
690 *Phys. Eng. Sci.*, 375, 20160318, doi: 10.1098/rsta.2016.0318, 2017.
- Weaver, A. J., Eby, M., Wiebe, E. C., Bitz, C. M., Duffy, P. B., Ewen, T. L., Fanning, A. F., Holland,  
M. M., MacFadyen, A., Matthews, H. D., Meissner, K. J., Saenko, O., Schmittner, A., Wang, H.,  
and Yoshimori, M.: The UVic earth system climate model: Model description, climatology, and



695 applications to past, present and future climates, *Atmosphere-Ocean*, 39, 361–428, doi:  
10.1080/07055900.2001.9649686, 2001.

Withers, P. J. A., and Jarvie, H. P.: Delivery and cycling of phosphorus in rivers: A review, *Sci. Total Environ.*, 400, 379–395, doi: 10.1016/j.scitotenv.2008.08.002, 2008.



700 **Tables:**

705 **Table 1: Overview of simulations. P fluxes are given in  $\text{TmolP a}^{-1}$ . In the P weathering simulations, only weathering anomalies were applied. In the P burial simulations, a constant P weathering flux ( $W_{P,0}$ ) balances P burial ( $BUR_P$ ) during the spin-up simulations. The preindustrial P inventory is identical in all simulations. More detailed information can be found in the text.**

Simulations	Abbreviation	Fluxes	P Burial parametrization
Reference (constant P inv.)	<i>Ref</i>	No	No burial
Anthropogenic P input	<i>Anthr</i>	Flux from Filippelli (2008)	No burial
Weathering	<i>Weath0.05</i>	$W_{P,0}=0.05$	No burial
Weathering	<i>Weath0.10</i>	$W_{P,0}=0.10$	No burial
Weathering	<i>Weath0.15</i>	$W_{P,0}=0.15$	No burial
Weathering	<i>Weath0.38</i>	$W_{P,0}=0.38$	No burial
Burial Reference	<i>Bur</i>	$BUR_P$ ( $t=1775a$ )=0.38 $W_{P,const}=0.38$	$r_{C:P}$ (Wallmann, 2010), C Burial (Flögel et al., 2011)
Burial Dunne	<i>Bur_Dun</i>	$BUR_P$ ( $t=1775a$ )=0.25 $W_{P,const}=0.25$	$r_{C:P}$ (Wallmann, 2010), C Burial (Dunne et al., 2007)
Low burial estimate	<i>Bur_low</i>	$BUR_P$ ( $t=1775a$ )=0.21 $W_{P,const}=0.21$	<i>Bur</i> configuration, but with $Y_F=100.5$ ; $A=90$ ; $r=38$ in (3)
High burial estimate	<i>Bur_high</i>	$BUR_P$ ( $t=1775a$ )=0.60 $W_{P,const}=0.60$	<i>Bur</i> configuration, but with $Y_F=167$ ; $A=108.5$ ; $r=29.5$ in (3)
Burial with restricted reservoir	<i>Bur_res</i>	$BUR_P$ ( $t=1775a$ )=0.41 $W_{P,const}=0.41$	<i>Bur</i> configuration, but with 113 $\mu\text{molP cm}^{-2}$ Reservoir
Burial without subgrid bathymetry	<i>Bur_noSG</i>	$BUR_P$ ( $t=1775a$ )=0.09 $W_{P,const}=0.09$	<i>Bur</i> configuration, but without subgrid bathymetry



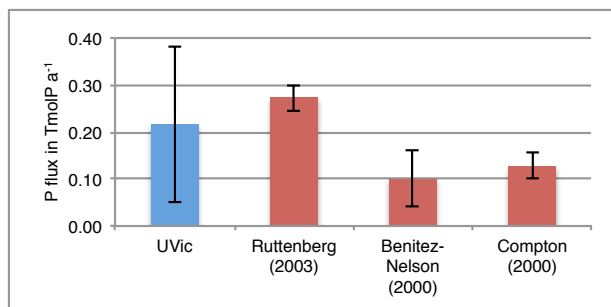
710 **Table 2: Rain rate of particulate organic carbon ( $RR_C$ ) to the seafloor for the shelf, slope and deep-sea areas from the observational estimate by Bohlen et al. (2012) and for the UVic model simulation *Bur* with and without subgrid bathymetry. Preindustrial  $RR_C$  shows no significant differences among all model simulations (except for simulation *Bur\_noSG*).**

		Bohlen (2012)			UVic model with subgrid bath. (Simulation <i>Bur</i> )			UVic model without subgrid bath. (Simulation <i>Bur_noSG</i> )		
	Depth [m]	$RR_C$ [TgC a <sup>-1</sup> ]	$RR_C$ [%]	Area [%]	$RR_C$ [TgC a <sup>-1</sup> ]	$RR_C$ [%]	Area [%]	$RR_C$ [TgC a <sup>-1</sup> ]	$RR_C$ [%]	Area [%]
Shelf	0-200	1056	60	6	1039	70	6.5	179	28	2.3
Slope	200-2000	393	22	10	205	14	11.7	219	34	13.3
Deep sea	>2000	312	18	84	235	16	81.9	238	37	84.6
Sum		1761			1479			637		

715



Figures:



720 Fig. 1: Globally integrated preindustrial P weathering fluxes in TmolP a<sup>-1</sup> from field studies (red) and the range of preindustrial P weathering fluxes covered by all simulations (blue with bars indicating the range; see  $W_{p,0}$  in Table 1). Estimates from field studies are based on literature values for global fluvial fluxes of bioavailable P and the error bars denote upper and lower limits of these estimates.

725

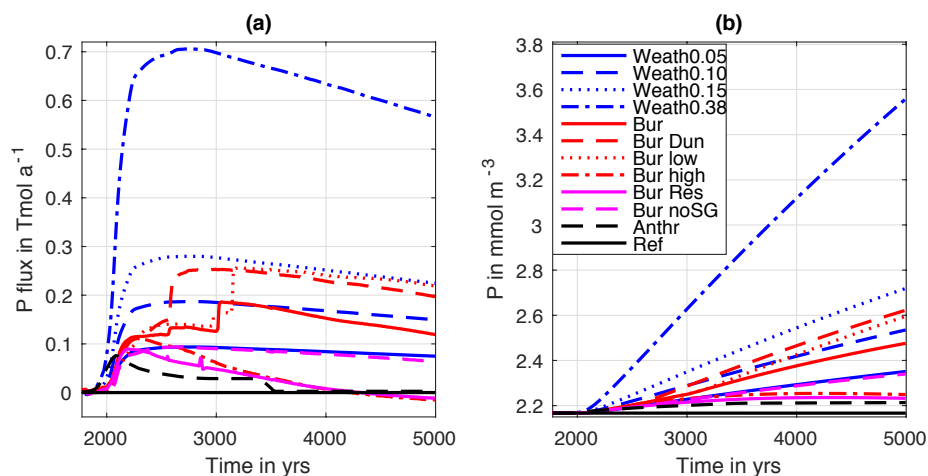
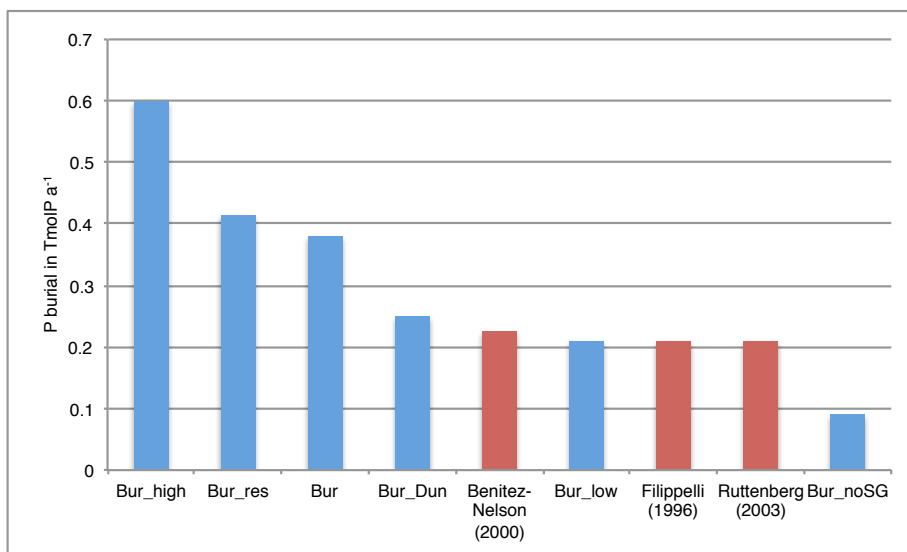
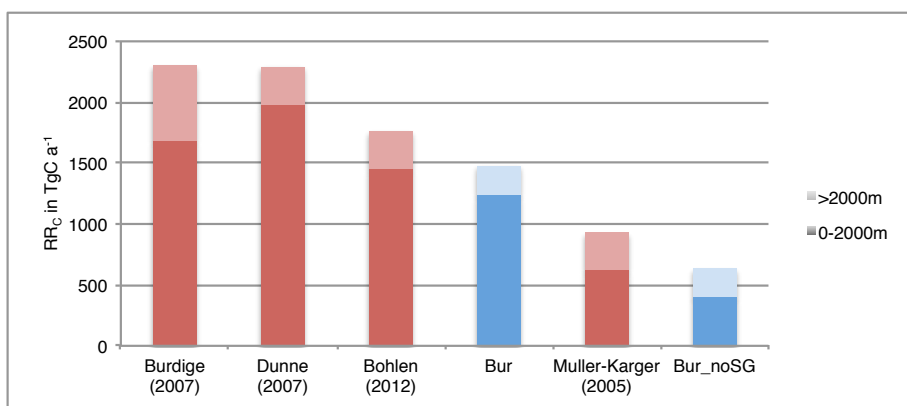


Fig. 2: (a) Globally integrated flux of P in Tmol a<sup>-1</sup> to the ocean and (b) globally averaged phosphate concentration in mmol m<sup>-3</sup>. Simulation descriptions can be found in Table 1.



730 **Fig. 3: Globally integrated preindustrial P burial fluxes in TmolP a<sup>-1</sup> from field studies (red) and for UVic model simulations in year 1775 (blue). Description of the model simulations can be found in Table 1.**



735 **Fig. 4: Globally integrated preindustrial rain rate of particulate organic carbon (RR<sub>c</sub>) to the seafloor in TmolC a<sup>-1</sup> from published studies (red) and for UVic model simulations (blue) between 0 to 2000m water depth (dark blue) and below 2000m (light blue). The simulation *Bur* is representative for all UVic model simulations except *Bur\_noSG*.**

740

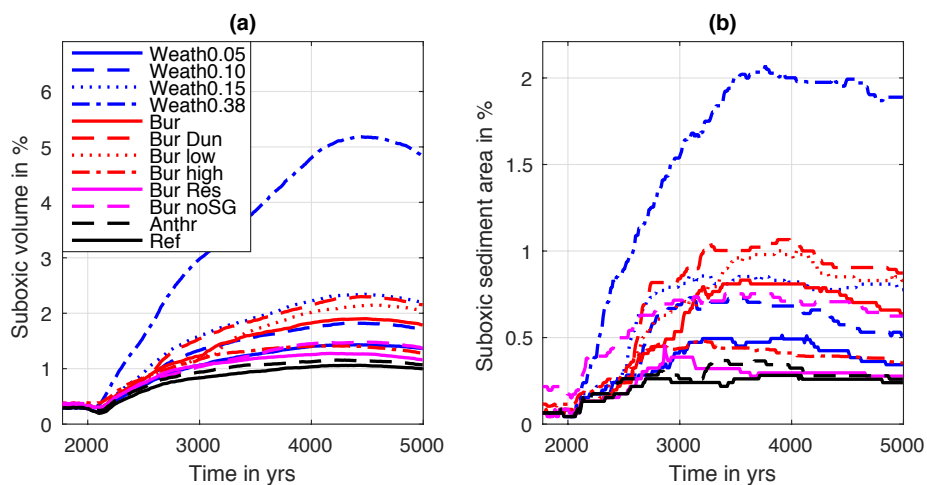


Fig. 5: Globally integrated (a) suboxic volume in percentage of total ocean volume and (b) suboxic sediment surface area in percentage of total sediment surface area. Water is designated as suboxic for oxygen concentrations below  $5 \text{ mmolO}_2 \text{ m}^{-3}$ . Simulation descriptions can be found in Table 1.

745

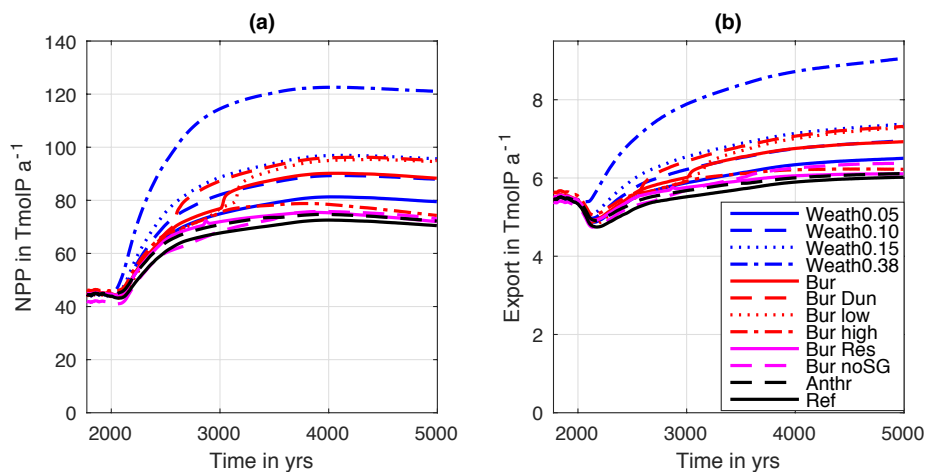


Fig. 6: Globally integrated (a) ocean net primary production (NPP) in  $\text{TmolP a}^{-1}$  and (b) export of organic P below the 130m depth level in  $\text{TmolP a}^{-1}$ . Simulation descriptions can be found in Table 1.

750

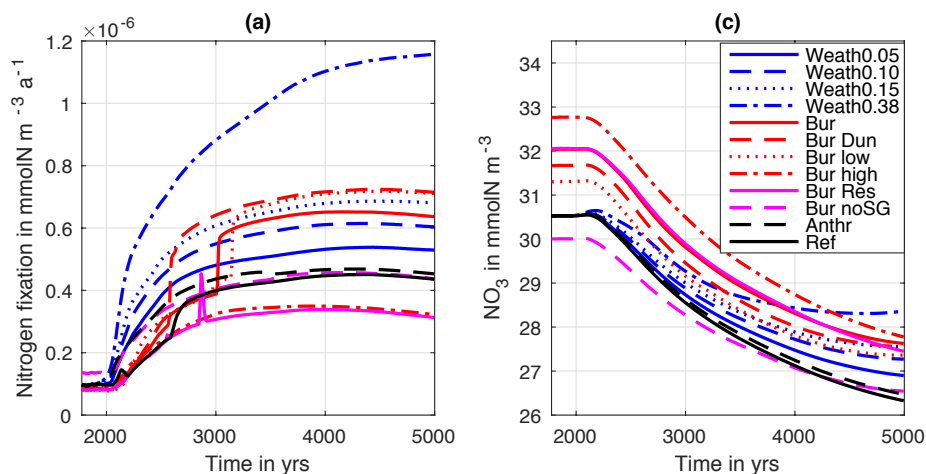
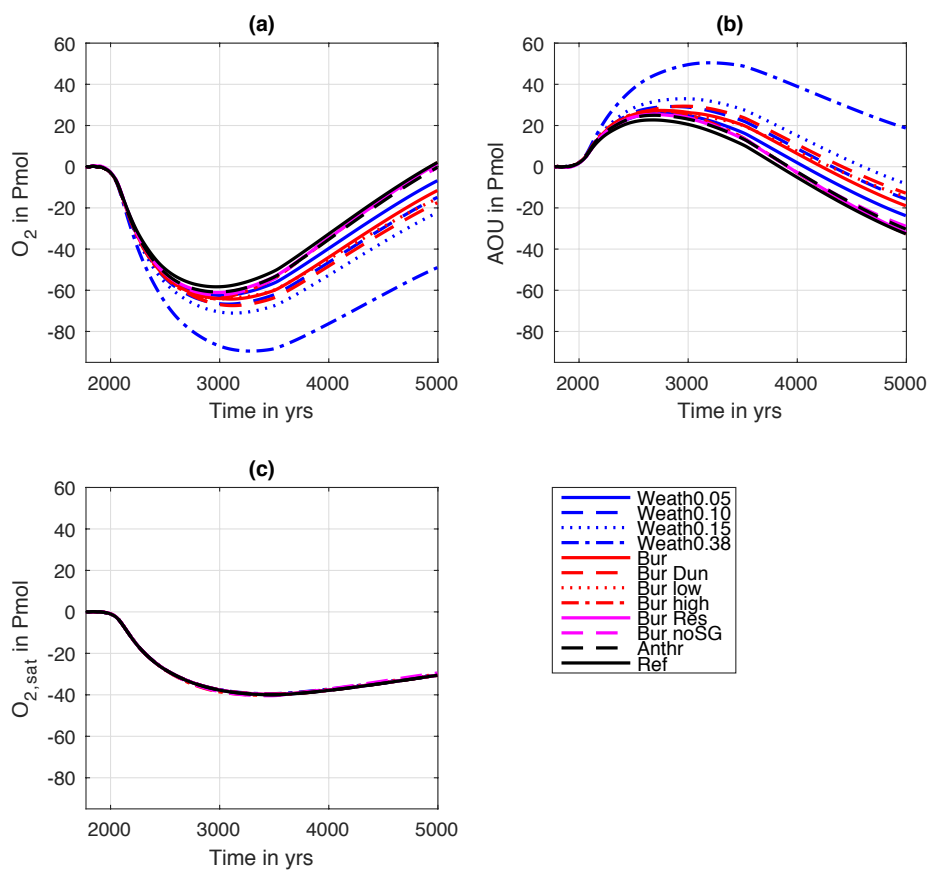
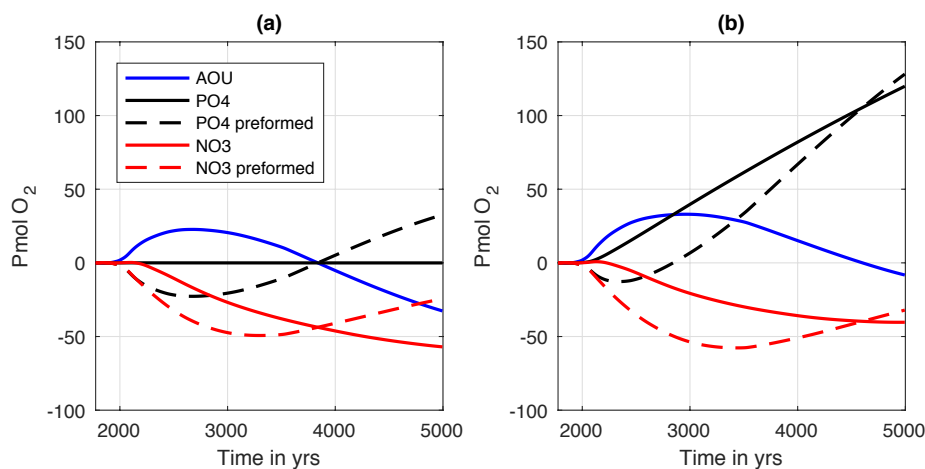


Fig. 7: Globally averaged (a)  $\text{N}_2$ -fixation in  $\text{mmolN m}^{-3} \text{a}^{-1}$  and (b)  $\text{NO}_3^-$  concentration in  $\text{mmolN m}^{-3}$ . Simulation descriptions can be found in Table 1.

755



**Fig. 8: Anomalies of globally integrated (a) O<sub>2</sub> content, (b) apparent oxygen utilization (AOU) and (c) oxygen saturation (O<sub>2,sat</sub>) in Pmol O<sub>2</sub>. Simulation descriptions can be found in Table 1.**



765

**Fig. 9:** Anomalies of globally integrated AOU (blue line),  $\text{PO}_4^{3-}$  (black solid line), preformed  $\text{PO}_4^{3-}$  (black dashed line),  $\text{NO}_3^-$  (red solid line) and preformed  $\text{NO}_3^-$  (red dashed line) expressed in  $\text{Pmol O}_2$  equivalents using constant elemental ratios (O:N=10 and O:P=160) for the (a) *Ref* simulation and the (b) *Weath0.15* simulation. Preformed nutrients are calculated as the difference between remineralized and total nutrient content. The calculations assume that all ocean water leaves the surface layer saturated in  $\text{O}_2$ .